P
A
C

Preparation and characterization of Fe-doped TiO$_2$ powders for solar light response and photocatalytic applications

Ibram Ganesh*, Polkampally P. Kumar, Abhishek K. Gupta, Panakati S.C. Sekhar, Kalathur Radha, Gadhe Padmanabham, Govindan Sundararajan

Laboratory for Photoelectrochemical (PEC) Cells and Advanced Ceramics, International Advanced Research Centre for Powder Metallurgy and New Materials (ARCI), Balapur PO, Hyderabad-500005, A.P., India

Abstract

Different amounts of Fe-doped TiO$_2$ (with 0.1 to 10 wt.% Fe) powders were prepared at temperatures in the range of 400 and 800 °C following a conventional co-precipitation technique and were thoroughly characterized by means of X-ray diffraction (XRD), Fourier-transform infrared (FT-IR), Fourier-transform Raman (FT-Raman), diffuse reflectance spectroscopy (DRS), BET surface area, zeta potential and flat band potential measurements. Photocatalytic ability of Fe-doped TiO$_2$ powders was evaluated by means of methylene blue (MB) degradation experiments conducted under the irradiation of simulated solar light. Characterization results suggested that as a dopant Fe stabilized TiO$_2$ in the form of anatase phase, reduced its band gap energy and adjusted its flat band potentials in such a way that these powders can be employed for photoelectrolysis of water into hydrogen and oxygen in photoelectrochemical (PEC) cells. The 0.1 wt.% Fe-doped TiO$_2$ exhibited highest activity in the photocatalytic degradation of MB. The kinetic studies revealed that the MB degradation reaction follows the Langmuir-Hinshelwood first order reaction rate.

Keywords: titania, doping, photocatalysis, band gap energy, semiconductor

I. Introduction

Recently, the photoelectrochemical (PEC) conversion of CO$_2$ to methanol and the photo-electrolysis of water into hydrogen and oxygen have received a great deal of attention from the scientific community as these two reactions can indeed harvest solar energy in the form of chemical energy [1–5]. These reactions are popularly called as artificial photosynthesis reactions, which require thermodynamic energy inputs of 1.5 and 1.23 eV, respectively [4–9]. Greater energy inputs are required to make up for losses due to band bending (necessary in order to separate charge at the semiconductor surface), resistance losses, and overvoltage potentials. The most frequently studied material for photoelectrode is TiO$_2$ [6,7]. Despite its high band gap energy of 3 eV, TiO$_2$ is the most preferred photo-electrode owing to its high photo-corrosion re-sistance in aqueous media, chemical stability, low cost and non-toxicity. Given its indirect band gap transition, the anatase in comparison to rutile and brookite phases of TiO$_2$ is the most preferred phase for photo-electrode applications. The maximum value obtained for the photovoltage of a PEC cell equipped with a TiO$_2$ photoanode is ~0.7–0.9 eV [10]. This implies that the PEC cell containing TiO$_2$ based single photoelectrode requires some amount of an external bias voltage to perform water oxidation reaction [1–10]. It is known that as long as external bias voltage or energy that is generated from fossil fuels is involved the artificial photosynthesis process performed in a PEC cell cannot be declared successful [11,12]. However, for the first time, Nozik [11,12] successfully photooxidized water into hydrogen and oxygen by utilizing simultaneously *n*-type TiO$_2$ as photoanode and *p*-GaP as photocathode without employing any external bias voltage in a PEC cell. Although Nozik's process was not successful commercially as *p*-GaP undergoes photocorrosion in aqueous based PEC cells, it demonstrat-

* Corresponding author: tel: +91 40 24442699,
e-mail: *ibramganesh@arci.res.in*

ed that given a stable *p*-type semi-conducting material with suitable band gap energy and band edges (i.e., flat band potentials), the water oxidation reaction (i.e., the energy consuming, endothermic, uphill and light reaction of natural photosynthesis) can be performed in a PEC cell without the need of any external bias voltage [11,12]. Since, TiO_2 is an excellent photoelectrode material with band edges suitable for water oxidation reaction, several efforts were made to convert *n*-type semi-conducting behaviour of TiO_2 into *p*-type, and also to reduce its band gap energy and the recombination of its photogenerated electron-hole pairs so that it can absorb a larger portion of sunlight that reaches the surface of the earth [4,8,13–23]. Thus, synthesis of *p*-type semi-conducting TiO_2 is of great importance from the point of view of artificial photosynthesis.

The *p*-type semi-conducting behaviour has been observed for TiO_2 that was doped with certain metal ions such as, Fe^{3+}, Co^{3+}, Ni^{2+}, Cu^+, etc. [4,8,13–23]. The change in the nature of semi-conducting behaviour of TiO_2 has been attributed to the hetero-unions formed between *n*-type TiO_2 and *p*-type doped metal oxide [4,8,13–23]. Among the various *p*-type semi-conducting materials, the Fe_2O_3 has been identified as a promising one as it possesses a considerably low band gap energy (E_{bg} = 2.2 eV) and the ionic radius of Fe^{3+} (0.64 Å) is quite comparable to that of Ti^{4+} (0.68 Å). However, Fe_2O_3 was found to be more prone to photocorrosion and the lifetime of its photogenerated minority carriers was found to be quite short [24]. In order to bring together the beneficial properties of Fe_2O_3 and TiO_2, the composites of these two semi-conducting oxides were prepared [16–23] and employed for photoassisted reduction of dinitrogen to ammonia, and the photoassisted degradation of waste materials in environment treatment [25,26]. The increase of Fe concentration from 0.2 to 0.5% in TiO_2 has resulted in the increased photocatalytic activity of the latter material prepared at 500 °C. However, when Fe content and calcination temperatures were further increased, the photocatalytic activity was found to decrease. This decrease was attributed to the limited solubility of Fe in TiO_2 (anatase or rutile), which is less than 1 wt.%. Furthermore, the hematite (α-Fe_2O_3) or pseudobrookite (Fe_2TiO_5) phases formed upon doping of >1 wt.% Fe were found to be responsible for the transfer of photogenerated charge carriers from TiO_2 to Fe_2O_3 (or Fe_2TiO_5) that resulted in the decreased photocatalytic activity [16–23]. In 1995, Tsodikov *et al.* [21] reported the formation of solid solutions of $Fe_x(Ti)_{1-0.75x}O_{2-\delta}$; 0.01<*x*<0.14. In another study, Wang, *et al.* [22] prepared Fe-doped TiO_2 (with 0.5 to 20 wt.% Fe) nanoparticles under different pH conditions following a hydrothermal method and found several differences in the structure and morphology of the resultant powders. At pH 1.8, anatase, brookite and trace of hematite together with a non-uni-

formly distributed Fe in the powder particles were noted upon doping with 0.5 wt.% Fe. This non-uniformity was attributed to the differences in the hydrolysing pH conditions of Fe and Ti precursors involved. Further, Fe was not detected in smaller particles as it could have been entered into the solid solutions of Fe-Ti oxides besides forming α-Fe_2O_3 particles. At pH 3.6, the phases of products were similar to those formed at pH 1.8, but the Fe distribution was slightly different from the previous one. In the samples prepared at pH 1.8, Fe was not detected in smaller particles, while in the samples prepared at pH 3.6, a plenty of Fe was detected, indicating that the distribution of Fe was more uniform at pH=3.6 conditions. At pH=6.0, the results showed only anatase phase for those powders doped with 20 wt.% Fe and a uniform solid solution of Fe-Ti oxides. The measurement of photocurrent at different electrode potentials showed the phenomena of *p-n* photoresponse coexistence. For higher contents of Fe doped samples, the smaller was the photocurrent, and the more positive was the conversion potential for samples prepared at pH=6.0. On the other hand, at higher pH, the larger was the photocurrent and the more positive was the conversion potential for powders containing the same amount of Fe. Yet in another study, Ranjit and Viswanathan [27] prepared Fe (0.11 to 1.76 wt.%) doped TiO_2 powders at 550 °C for 24 h following a conventional co-precipitation and the sol-gel technique. The anatase to rutile phase transformation was found to be dependant on the nature of the precursor involved. Sol-gel-derived Fe-doped TiO_2 catalysts showed the presence of rutile and pseudobrookite phases, whereas, the coprecipitated catalysts showed only the anatase phase. The role of the dopant ion was primarily to improve the charge separation of the photoproduced electron-hole pairs *via* a permanent electric field. The photocatalytic activity of the Fe-doped TiO_2 catalysts has been explained in terms of the heterojunction formed between the Fe/TiO_2 and α-Fe_2O_3 phases for the sol-gel-derived catalyst. An increase in dopant ion content was found to favour the electron-hole separation and therefore the photoactivity. However, beyond a certain level, the space charge layer became thicker, and the probability of carrier recombination increased. Thus, there is an optimal value at which the photoactivity reaches a maximum.

In some other studies, the structural and electrical properties of Fe-doped TiO_2 thin films have also been studied [16–22]. In a study, Ballyy *et al.* [23] prepared different amounts of Fe-doped TiO_2 thin films under identical conditions. Doping of Fe has induced a structural transformation from anatase at low Fe concentration to rutile for the concentrations of >0.32 at.% Fe. The electrical and thermoelectric power measurements indicated that the electrical conduction changed from *n*-type conduction for undoped TiO_2 to *p*-type

conduction for heavily doped TiO$_2$, and demonstrated that Fe atoms behaved as an acceptor impurities. Even at high Fe concentration, thin films remained transparent. The highest *p*-type conductivity reached at room temperature was about 10^{-6} S/m [23]. The dispersion of the permittivity with frequency indicated that the electrical conduction of the thin films was inhomogeneous. The influence of the Fe atom was found to depend on the crystal structure of the oxide. It was also found that the introduction of Fe generated more oxygen vacancies in anatase than in rutile. A large fraction of the acceptors created by the Fe atoms were found to be compensated by the oxygen vacancies created by the same Fe atoms. In addition to these, it was also found that pure rutile and Fe-doped TiO$_2$ had higher *p*-type conductivity than mixed, anatase/rutile TiO$_2$ thin films doped with Fe. Yet in another study, Singh *et. al.* [28] prepared nanostructured Fe-doped TiO$_2$ thin films by sol-gel spin coating method for photoelectrochemical studies. XRD study showed that the films were polycrystalline with the photoactive anatase phase of TiO$_2$. Doping of Fe in TiO$_2$ resulted in a shift of absorption edge towards the visible region of solar spectrum. The observed band gap energy decreased from 3.3 to 2.89 eV on increasing the Fe doping concentration from 0 to 0.2 at.%. The 0.2 at.% Fe-doped TiO$_2$ exhibited the highest photocurrent density of about 0.92 mA/cm^2 at zero external bias. Flat band potential and donor density determined from the Mott–Schottky plots were found to vary with doping concentration from -0.54 to -0.92 V/SCE and 1.7×10^{19} to 4.3×10^{19} cm^{-3}, respectively. Although, many published articles deal with Fe-doped TiO$_2$ materials, there is contradicting information as far as the effect of Fe-doping on photo-current and photo-catalytic behaviour of TiO$_2$ is concerned [16–23]. Further, the information on photo-current and flat band potential properties of Fe-doped TiO$_2$ materials is not sufficiently reported. Furthermore, the structure-property-performance correlation of Fe-doped TiO$_2$ powders is hardly presented and discussed in the literature and the information pertaining to degradation of methylene blue (MB) over Fe-doped TiO$_2$ powders under the irradiation of the light that is equivalent to the solar light reaching the surface of the earth is not available.

In view of the above, different amounts of Fe-doped TiO$_2$ powders were prepared following a conventional co-precipitation method, calcined in air and were characterized following various techniques such as, XRD, SEM, EDAX, FT-IR, FT-Raman, DRS, BET surface area, zeta potential, flat band potential, photocatalytic activity, band gap energy value measurements, etc., and thus obtained results are presented and discussed in this paper to reveal the effects of Fe-doping on solar light induced response and photocatalytic behaviour of TiO$_2$.

II. Experimental

2.1 Synthesis of Fe-doped TiO$_2$ powders

Different amounts of Fe-doped TiO$_2$ (with 0, 0.1, 0.2, 0.3, 0.4, 0.5, 0.6, 0.7, 0.8, 0.9, 1, 2, 3, 4, 5, 6, 7, 8, 9 and 10 wt.% Fe) powders were prepared by following a conventional co-precipitation technique using ammonium hydroxide as an hydrolyzing agent [29,30]. The concentration of Fe in the prepared powders is expressed in terms of atomic weight percent in throughout this paper unless otherwise mentioned. In a typical experiment, cold titanium tetrachloride (TiCl$_4$, Fluka, AR grade) was first digested in cold concentrated HCl (AR Grade, Loba Chemie, Mumbai, India) and was subsequently diluted with deionized water. To this solution, the requisite amount of iron nitrate (Fe(NO$_3$)$_2$×6H$_2$O, AR Grade, Loba Chemie, Mumbai, India) was added after dissolving separately in deionized water. The resultant solution was hydrolyzed by adding the 50% diluted solution of ammonium hydroxide drop by drop until the complete precipitate (at pH≈9) was obtained. This precipitate was heated for about 12 h at 90 °C to facilitate the aging process. The resultant precipitate was filtered off and washed thoroughly with doubly distilled water until no chloride ions could be detected with Ag$^+$ ions in the filtrate. Thus obtained Fe(OH)$_3$–Ti(OH)$_4$ coprecipitate was then oven dried at 120 °C for 24 h and calcined at 550 °C for 6 h in an open-air atmosphere using an electrical muffle furnace. Some portions of the dried precipitates were also separately calcined at 400, 500, 600, 700 and 800 °C for 6 h in order to evaluate the thermal stability of these powders.

2.2 Photocatalytic activity evaluation

The photocatalytic activity of Fe-doped TiO$_2$ powders was evaluated by performing methylene blue (MB) (Loba-Chemie, Mumbai, India) degradation experiments under the irradiation of a simulated solar light. In a typical experiment, about 200 mL of 0.01, 0.02 or 0.03 mM aqueous MB solution and 0.24 g fine powder catalyst were taken in a glass dish of 150 mm diameter × 75 mm height (Borosil, India) and was exposed to simulated solar light (Osram 1000 W Xenon short arc display/optic lamp, XBO, Germany, installed in a light-condensing lamp housing, Model No.: SS-1K, Sciencetech Inc., Canada) for different time intervals (up to 4 h). Before irradiation the incident light was passed through an AM1.5G air-mass filter so that the intensity of the incident light measured about 44.42 mW/cm^2 [31]. The reaction mixture solution was initially stirred for about 2 h in the dark in order to reach the adsorption equilibrium. During light irradiation, the reaction mixture was continuously stirred using a magnetic stirrer (Model: 5MLH, Remi, Mumbai, India) and aliquots of the reaction mixtures were collected at regular time intervals to monitor the re-

action progress. The leftover MB concentration in the reaction mixtures was estimated with the help of UV-Vis spectrophotometer (Lambda 650, Perkin Elmer, Massachusetts, USA). The maximum absorption peak (λ_{max}) of MB at about 666 nm was considered to estimate the remaining concentration of MB [31].

2.3 Flat band potential measurement

The electron energy states of quasi-Fermi levels ($_nE_F{}^*$) of Fe-doped TiO_2 (with 0.1, 0.5, 1, 5, and 10 wt.% Fe) powders were measured using methylviologen dichloride (MV^{2+}, $E_{red} = -0.445$ V vs. normal hydrogen electrode, NHE) as a pH-independent redox system [32,33]. The estimated pH_0 values were converted to the Fermi potentials (i.e., flat band potentials) at pH=7 by the equation $*E_{F(pH=7)} = -0.445 + 0.059 \cdot (pH_0 - 7)$. Reproducibility of the pH_0 values was better than 0.1 pH units. In a typical experiment, 30 mg of catalyst powder and 6 mg of MV^{2+} were suspended in a specially designed glass reactor cell having a flat quartz window (~75 mL of 0.1 M KNO_3). A platinum flag of 1 cm^2 area and Ag/AgCl were served as working and reference electrodes, respectively, and a pH meter was used for recording the proton concentration. Prior to measurements, the solutions were purged with argon gas (>200 mL/min) for >2 h and continued the same during voltage measurements. Initially, the pH of the solution was adjusted to pH=1–2 prior to recording the voltage readings using a solution of HNO_3 (0.1 M). The light source was a Xenon arc lamp of 500 W (Solar Simulator, Oriel 91160) having AM 1.5G filter and a monochromator (Newport-74125 model) with a bandwidth of 5 nm. Stable photovoltages were recorded after about 30 min of changing the pH value using a multi-meter (Agilent, Singapore) [32,33]. All the potentials presented here are against NHE reference.

2.4 Characterization

A Gemini Micromeritics analyzer (Micromeritics, Norcross, USA) was used for Brunauer-Emmett-Teller (BET) surface area measurements. The BET surface area was measured by nitrogen physisorption at liquid nitrogen temperature (–196 °C) by considering 0.162 nm^2 as the area of cross section of N_2 molecule. Prior to measurements, the samples were evacuated (up to 1×10^{-3} Torr) at 180 °C for 2 h. Phase analysis, crystallite size and lattice parameter values of the powders were determined by X-ray diffraction (Bruker's D8 advance system, Bruker's AXS, GmbH, Germany) using Cu Kα radiation source. To obtain quantitative information of phases, the most intense peak of the individual phase was taken into consideration. The peak heights of all the phases were summed up and the percentage concentration of a particular phase was estimated from the ratio of the strongest peak of that phase to the sum of various phases present in a system [34,35]. The crystallite sizes of the powders were estimated with the help of Debye-Scherrer equation ($<L>_{hkl} = K \cdot \lambda / \beta_{hkl} \cos\theta$; where K is a constant taken as 1 and β is the integral breadth that depends on the width of the particular hkl plane; $\lambda = 1.5406$ Å, the wavelength of the Cu Kα source; and θ is the Bragg's angle) using the XRD data of the strongest reflection of the major phase [34,35]. The lattice parameter values were determined using equation $1/d_{(hkl)}{}^2 = (h^2+k^2)/a^2 + l^2/c^2$ (where the value of $d_{(hkl)}$, for an XRD peak, was determined from Bragg's law, $2d_{(hkl)} \cdot \sin\theta = n \cdot \lambda$). Here, hkl is the crystal plane indices, $d_{(hkl)}$ is the distance between crystal planes of (hkl), and a, c are the lattice parameters (for tetragonal anatase and rutile phases of TiO_2: $a = b \neq c$). The planes, (101) and (200) for anatase (ICDD File No.: 03-065-5714), and the (110) and (211) for rutile (ICDD File No.: 03-065-1118) were considered while calculating the lattice parameters values. The content ratio of the anatase to rutile phase in titanium dioxide was roughly estimated using the following equations [36,37]:

$$C_A = 100 / (1 + 1.265 \, I_A/I_R) \qquad (1)$$

$$C_R = 1 - 100 / (1 + 1.265 \, I_A/I_R) \qquad (2)$$

where C_A is content ratio of anatase (%) and C_R content ratio of rutile (%).

The micrographs of the powders were examined using a scanning electron microscope (JSM–5410, JEOL, Japan) with an energy dispersive scanning (Sigma 3.42 Quaser, Kevex, USA) attachment for qualitative and quantitative micro analysis. The FT-IR spectra were recorded on an FT-IR 1650 Perkin–Elmer Spectrometer (4000–200 cm^{-1}) using KBr pellets. The FT-Raman spectra were recorded on a triple subtractive Jobin Yvon T64000 Raman spectrometer equipped with a liquid-nitrogen-cooled charge-coupled device (CCD) detector. Diffuse reflectance spectra (DRS) of the powders were recorded on a Shimadzu UVPC 3101 spectrophotometer equipped with an integration sphere. The powder samples were directly placed into a cylindrical sample port holder (3 cm diameter, 1 mm deep). The zeta-potentials of powders in 10^{-3} M KCl aqueous solutions were measured on a Zeta meter (Zeta Meter Inc., USA). The band gap energies of Fe-doped TiO_2 powders were calculated using the absorbance data obtained from DRS study following the Tauc's relation [$(\alpha \cdot h \cdot v) = C(h \cdot v - E_g)^n$], where C is a constant, α is absorption coefficient, E_g is the average band gap of the material and n depends on type of transition (2 for indirect band gap and ½ for direct band gap), h is the Plank's constant (6.626×10^{-34} J·s), v is the frequency of photons [38,39]. The direct and indirect average band gap transition energies were estimated from the intercepts of linear portion of the $(\alpha \cdot h \cdot v)^2$ or $(\alpha \cdot h \cdot v)^{1/2}$ vs. $h \cdot v$ of plots, respectively.

III. Results and discussion

X-ray diffraction patterns of the Fe-doped TiO_2 (with 0 to 0.9, and 1 to 10 wt.% Fe) powders formed at 550 °C for 6 h are presented in Fig. 1. For sake of an easy interpretation, the XRD patterns reported in ICDD files for anatase TiO_2 (ICDD File No.: 03-065-5714) and rutile TiO_2 (ICDD File No.: 03-065-1118) are also presented in these figures. It can be seen that, in general, all the powders are well crystalline materials. The pure un-doped TiO_2 is in the form of rutile and all the Fe-doped TiO_2 powders are mainly in anatase phase together with some minor phases including α-Fe_2O_3, $TiFeO_3$, and $Fe_x(Ti)_{1-0.75x}O_{2-\delta}$; $0.01 < x < 0.14$ [16–22]. Even 0.1 wt.% Fe-doping was sufficient to completely transform TiO_2 from rutile to anatase phase. Anatase is the only phase in the powders doped with Fe up to a concentration of 3.0 wt.%, and in the case of powders doped with 4 to 10 wt.%, in addition to anatase phase, the appearance of some minor XRD lines belong to hematite (α-Fe_2O_3) ($2\theta = 28.585°$), (006) plane and ilmenite, $TiFeO_3$ ($2\theta = 32.529°$), (003) plane are also seen [16]. The intensity of lines belonging to hematite is higher than that of ilmenite phase. The intensity of a XRD peak at $2\theta = 32.529°$ belong to $TiFeO_3$ was neither increased nor decreased linearly with the increasing concentration of Fe in TiO_2. The reason for this anomalous behaviour is yet to be fully understood. Even the 10 wt.% Fe doping could not transform TiO_2 completely from anatase to rutile phase even though the excess doped Fe

was converted into small amounts of hematite and ilmenite phases. However, these results are contradicting with one reported by Ballyy *et al*. [23]. In their study, even 0.32 wt.% Fe doping caused the transformation of TiO_2 from anatase to rutile phase in thin films. In another study, Ranjit and Viswanathan [27] noted the formation of rutile and pseudobrookite titania phases upon doping 0.11 to 1.76 wt.% Fe in TiO_2 formed by a sol-gel route. However, they have noted only anatase phase for the same amounts of Fe-doped TiO_2 powders formed in a conventional co-precipitation method. The different preparation methods and conditions adopted could be the reasons for observing such contradicting phase transformation results.

Figure 2 depicts the XRD patterns of the 5 wt.% Fe-doped TiO_2 powders formed at different temperatures ranging from 400 to 800 °C for 6 h. The powders formed at 400 and 500 °C are in the form of poorly crystalline anatase phase, whereas, the one formed at 600 °C is in a highly crystalline anatase phase. The powder formed at the latter temperature also contains some small amounts of hematite in addition to anatase phase. On further increase of calcination temperature to 700 °C, some amount of anatase phase was transformed into rutile phase. After calcination at 800 °C, about 95% of the powder was transformed into rutile phase. It is interesting to see that the powder formed at 800 °C does not contain any free hematite indicating that Fe could have been entered completely into TiO_2 crystal structure leading to the forma-
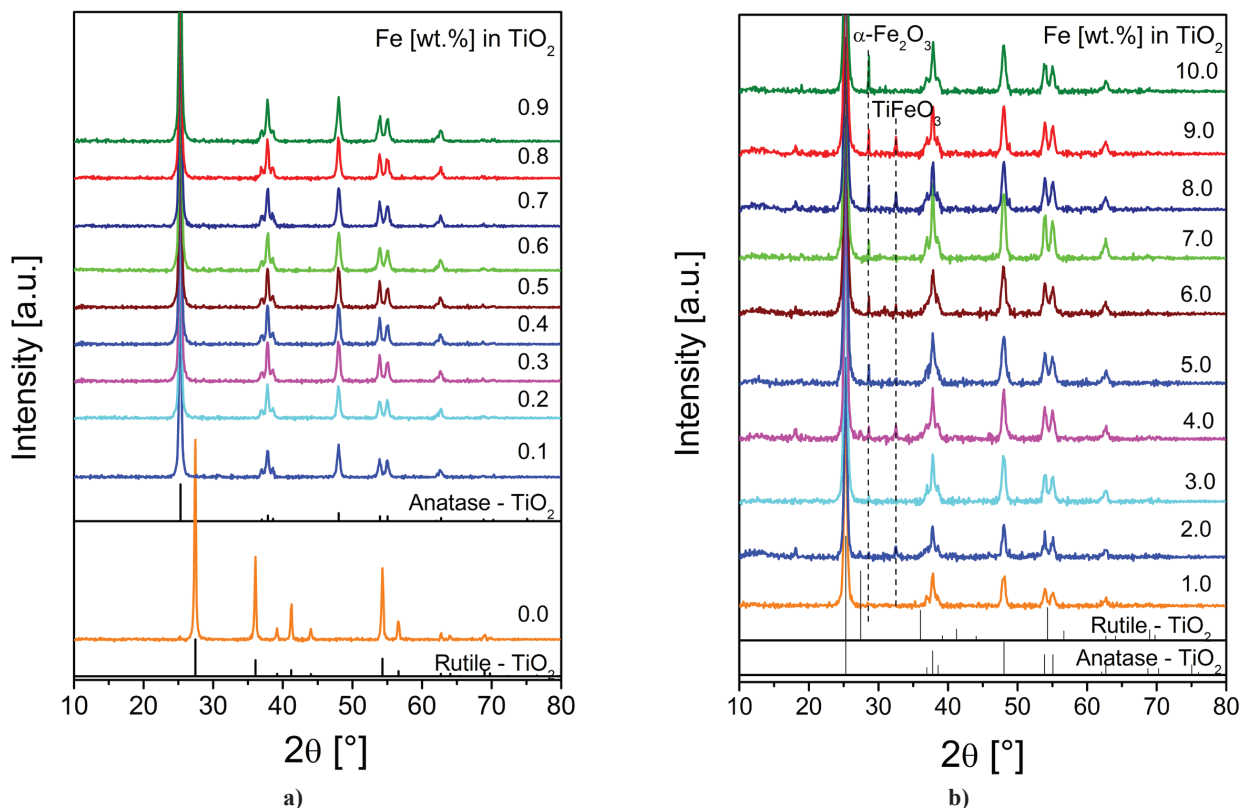

Figure 1. XRD patterns of Fe-doped TiO_2 powders (with 0 to 0.9 wt.% Fe (a), and 1 to 10 wt.% Fe (b)) formed at 550 °C for 6 h (rutile TiO_2: ICDD File No.: 03-065-1118; anatase TiO_2: ICDD File No.: 03-065-5714)
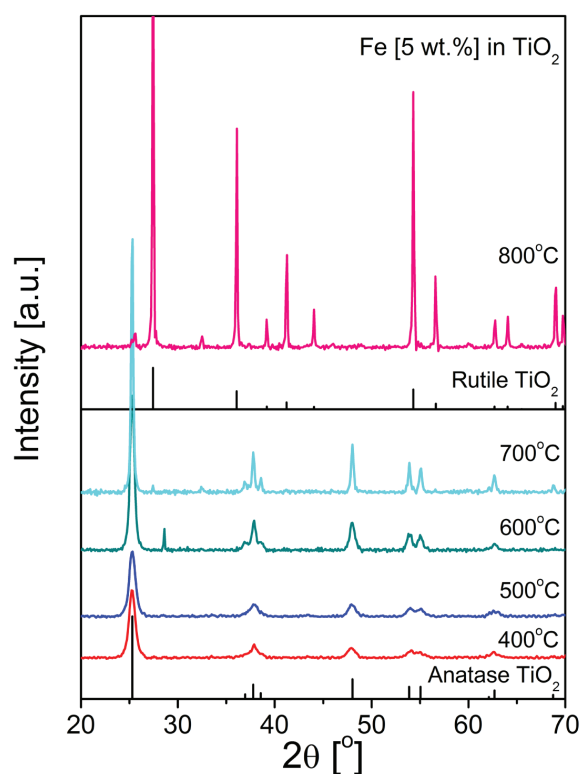
Figure 2. XRD patterns of 5 wt.% Fe-doped TiO₂ powder formed at 400 to 800 °C for 6 h (rutile TiO₂: ICDD File No.: 03-065-1118; anatase TiO₂: ICDD File No.: 03-065-5714)

tion of a solid-solution of Fe^{3+} in TiO_2 or it was highly dispersed as iron oxide on the surface of TiO_2. The almost similar ionic radius of Fe^{3+} (0.64 Å) to that of Ti^{4+} (0.68 Å) could be the reason for stabilizing TiO_2 in the form of anatase phase by replacing some portion of Ti^{4+} ions in TiO_2 lattice by Fe^{3+} [4,8,13−23]. Tsodikov *et al.* [21] also observed the formation of similar solid solutions of $Fe_x(Ti)_{1−0.75x}O_{2−\delta}$; $0.01<x<0.14$.

The thermogravimetry (TG) and differential scanning calorimetry (DSC) profiles of $Fe(OH)_3−Ti(OH)_4$ formed from the precursor mixtures of 0, 0.5, 1, 5 and

10 wt.% Fe-doped TiO_2 powders are presented in Fig. 3. A close look into these profiles reveals that all the weight losses occurred are associated with their corresponding thermal (exothermic or endothermic) events. From ambient to 400 °C there are two major weight losses with corresponding thermal events, which are attributed to the loss of physically adsorbed moisture and conversion of hydroxides into amorphous oxides, respectively. After 400 °C none of the materials underwent > 5% weight loss. Furthermore, with the increase of Fe-content in TiO_2, there is a gradual increase in the weight loss and in the corresponding endothermic nature below 400 °C. These events suggest that Fe-doping causes the increased absorption/adsorption of moisture by TiO_2 powders. Furthermore, these results unequivocally suggest that all the iron-doped TiO_2 powders are thermally quite stable between 400 and 1000 °C.

The values of BET surface area, crystallite size and lattice parameters of the Fe-doped TiO_2 (with 0, 0.1, 0.5, 1, 5, and 10 wt.% Fe) powders formed at 550 °C for 6 h are presented in Table 1. The average crystallite size and surface area of the undoped rutile TiO_2 powder are 17.82 nm and 23.25 m²/g, respectively. Upon doping with 0.1 wt.% Fe the crystallite size value decreased to 15.87 nm and the surface area increased to 65.92 m²/g. When dopant concentration was further increased gradually from 0.1 to 10 wt.%, both crystallite size and BET surface area values are gradually decreased reaching the values of 13.24 nm and 48.82 m²/g, respectively, for the 10 wt.% Fe-doped TiO_2. The decrease of crystallite size with the increase of Fe concentration in TiO_2 is quite expected as the ionic radius of Fe (0.64 Å) is relatively smaller than that of Ti (0.68 Å). On the other hand, the decrease of BET surface area with the increase of Fe in TiO_2 could be attributed to the increased particle size (i.e. agglomeration) of the powder. The increase of agglomeration with the increase of Fe in TiO_2 could be attributed to many reasons including the rela-
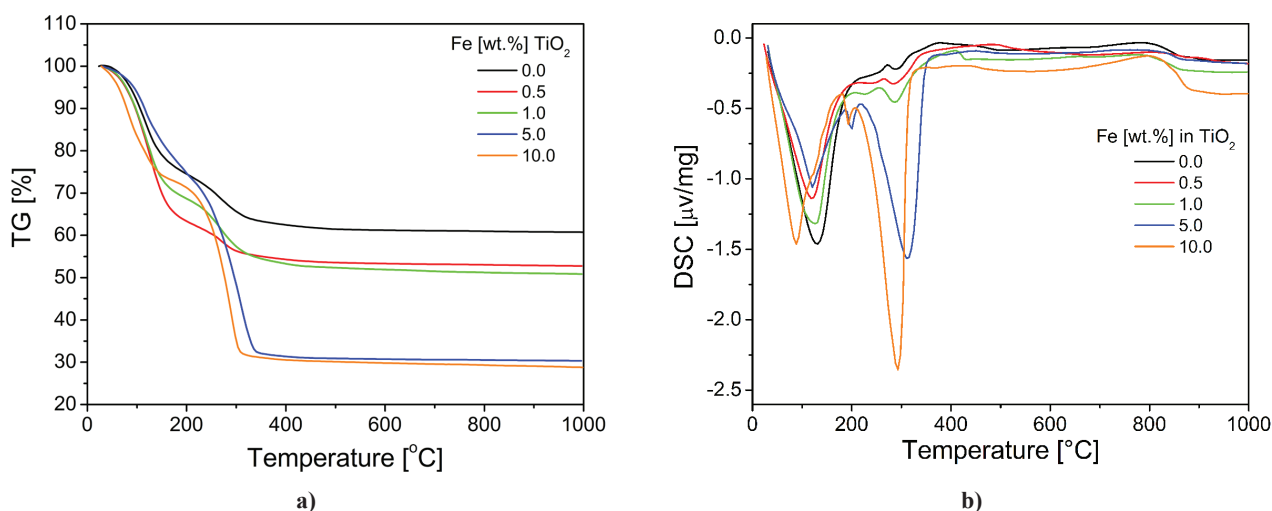

a)

b)

Figure 3. The profiles of: a) thermogravimetry, TG and b) differential scanning calorimetry, DSC, of hydroxides formed out from precursor mixtures of 0, 0.5, 1, 5 and 10 wt.% Fe-doped TiO₂ powders

Table 1. BET surface area, crystallite size and lattice parameter values of 0, 0.1, 0.5, 1, 5 and 10 wt.% Fe-doped TiO$_2$ powders formed at 550 °C for 6 h[†]

Fe in TiO$_2$ [wt.%]	BET surface area [m²/g]	Crystallite size [nm]	Lattice parameter [Å]	
			$a (= b)$	c
0.0	23.25	17.82	4.585	2.964 (rutile)
0.1	65.92	15.87	3.785	9.717 (anatase)
0.5	65.59	15.13	3.792	9.713 (anatase)
1.0	61.92	14.43	3.785	9.626 (anatase)
5.0	60.71	13.78	3.785	9.457 (anatase)
10.0	48.82	13.24	3.785	9.424 (anatase)

[†]The values are arrived as detailed in the experimental section
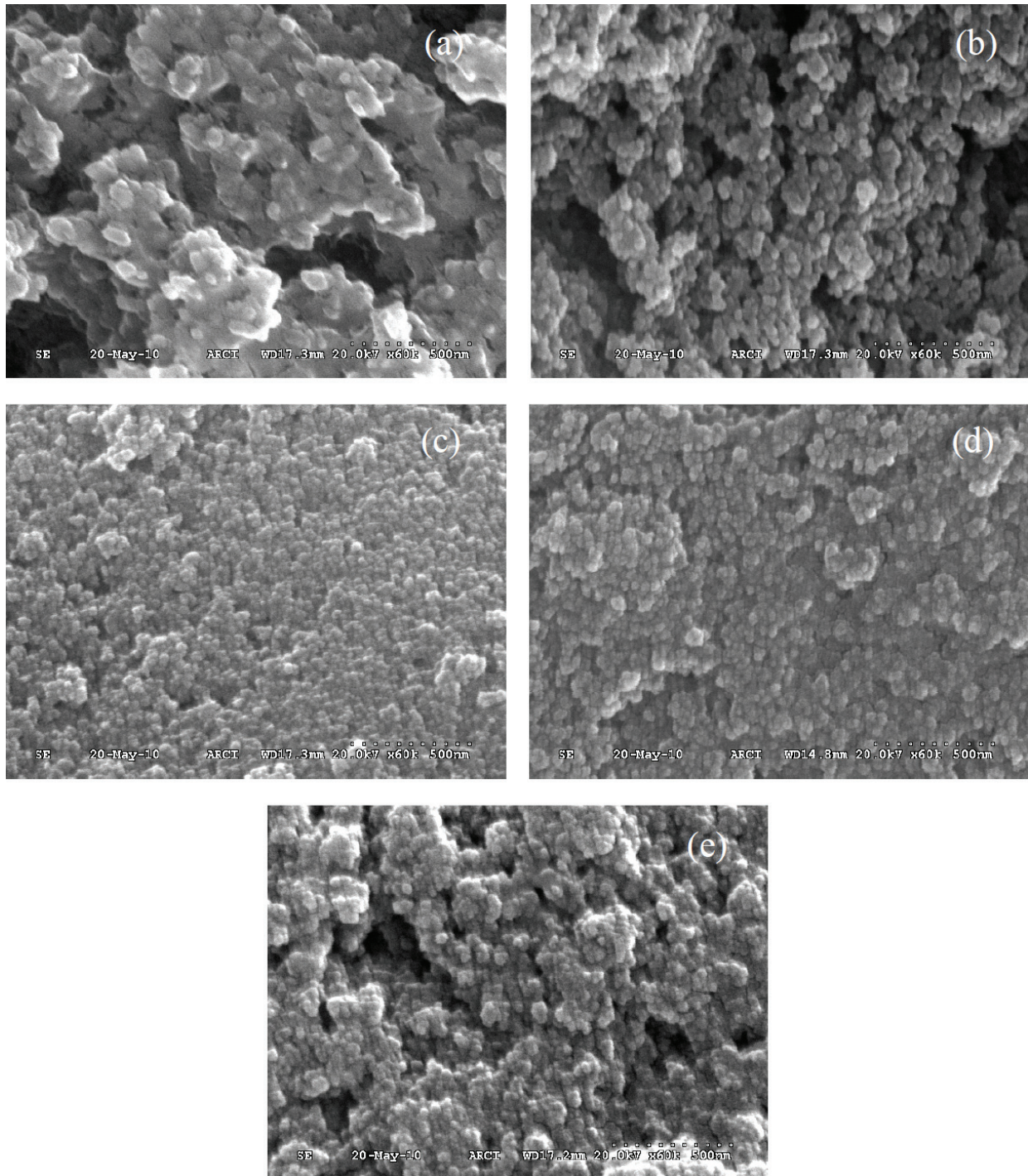

Figure 4. SEM micrographs of Fe-doped TiO$_2$ powders with: a) 0, b) 0.1 c) 0.5 d) 1 and e) 10 wt.% Fe, formed at 550 °C for 6 h
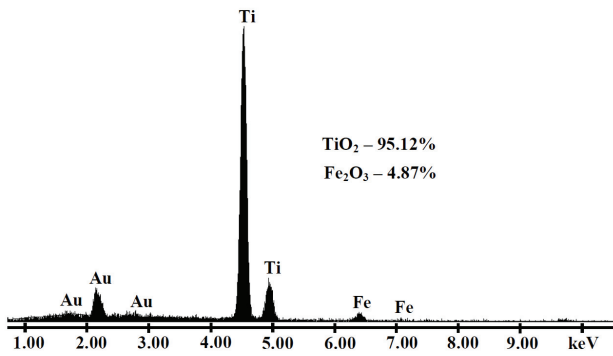
Figure 5. EDAX spectra of 5 wt.% Fe-doped TiO$_2$ powder formed at 550 °C for 6 h

tively lower melting point of Fe$_2$O$_3$ (1566 °C) than that of TiO$_2$ (1843 °C). The *a* and *c* lattice constant values estimated for undoped TiO$_2$ are 4.585 Å and 2.964 Å, respectively, whereas those estimated for anatase powders (i.e. for TiO$_2$ powders doped with 0.1, 0.5, 1, 5 and 10 wt.% Fe) are not varied much with the increase of Fe dopant concentration in TiO$_2$. The value noted for *a* parameter is 3.785 Å for all the powders, whereas, the *c* parameter value changed from 9.717 to 9.424 Å when iron concentration was increased from 0.1 to 10 wt.%. These lattice parameter values suggest that Fe-doping causes the decrease of TiO$_2$ crystallite size along *c*-axis as the ionic radii of Fe (0.64 Å) is relatively smaller than that of Ti (0.68 Å). Nevertheless, these estimated lattice parameter values are well comparable with those reported for rutile TiO$_2$ (ICDD File No.: 03-065-1118),
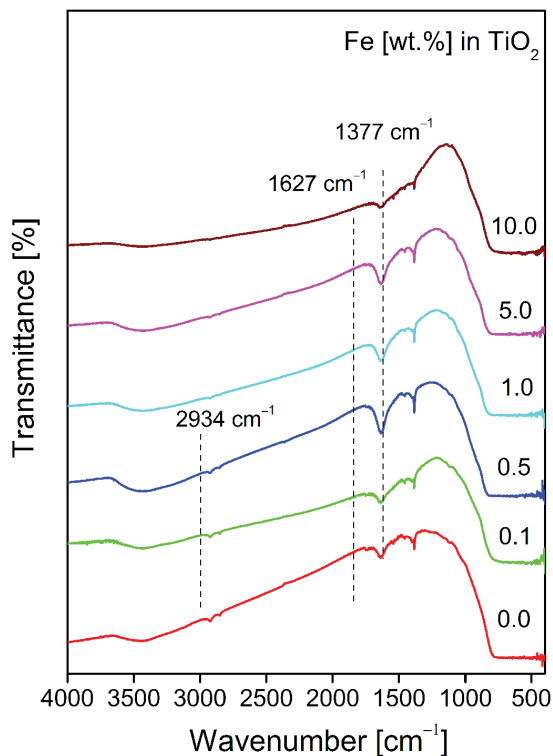

Figure 6. FT-IR spectra of Fe-doped TiO$_2$ (with 0, 0.1, 0.5, 1, 5 and 10 wt.% Fe) powders formed at 550 °C for 6 h

anatase TiO$_2$ (ICDD File No.: 03-065-5714), and Fe-doped TiO$_2$ powders [4,8,13−23].

The SEM micrographs of the Fe-doped TiO$_2$ (with 0, 0.1, 0.5, 1 and 10 wt.% Fe) powders formed at 550 °C for 6 h are presented in Fig. 4. It can be seen that the morphology of the undoped TiO$_2$ powder is completely different from those of Fe-doped TiO$_2$ powders. In general, all the Fe-doped TiO$_2$ powders consist of nano-sized primary particles with spherical shape in agglomerated powder particles, whereas, the pure TiO$_2$ powder consists of relatively larger (micron size) chunks of powder particles. The primary particles of the 0.1 and 0.5 wt.% Fe-doped TiO$_2$ powders are finer (~50 nm) than those estimated for the 1 and 10 wt.% Fe-doped TiO$_2$ powders. The pure undoped TiO$_2$ powder consists of 1−3 μm sized agglomerates with almost fused primary particles of about 200 to 500 nm size. A close look into these powders' micrographs reveals that the degree of agglomeration initially decreased with the doping of 0.1 wt.% Fe into TiO$_2$ and after that it is gradually increased with the further increase of Fe content in TiO$_2$. In order to establish the achievement of the targeted chemical composition in the synthesized powders, the 5 wt.% Fe-doped TiO$_2$ powder was examined by EDAX analysis as depicted in Fig. 5. The chemical composition observed in EDAX analysis confirms that the targeted chemical composition (within allowed experimental errors) was achieved in the powders formed in a conventional co-precipitation method.

The FT-IR spectra of Fe-doped TiO$_2$ (with 0, 0.1, 0.5, 1, 5, and 10 wt.% Fe) powders calcined for 6 h at 550 °C are presented in Fig. 6. The presence of some weak transmittance bands between 3400 and 3600 cm^{-1} at 1627 cm^{-1} and at 1377 cm^{-1} are seen, which are gradually decreased with the increase of Fe concentration in TiO$_2$. These bands are attributed to the stretching vibrations of the O-H groups and the bending vibrations of the adsorbed water molecules, respectively [4,8,13−23]. A band between 650 and 830 cm^{-1} is seen which is attributed to different vibrational modes of TiO$_2$. Anatase and rutile phases of TiO$_2$ exhibit certain strong FT-IR absorption bands in the regions of 850−650 and 800−650 cm^{-1}, respectively [29,30]. The broad intense band seen below 1200 cm^{-1} is due to Ti-O-Ti vibrations [13−23]. These results match very well with those reported in the literature for Fe-doped TiO$_2$ powders and for anatase and rutile phases of TiO$_2$ [4,8,13−23].

Figure 7 shows the Raman scattering spectra of Fe-doped TiO$_2$ (with 0, 0.1, 0.5, 1, 5 and 10 wt.% Fe) powders formed for 6 h at 550 °C. The tetragonal rutile structure possesses two TiO$_2$ molecules in the unit cell with the space group $D_{4h}^{14}(P4_2/mnm)$ and the lattice constants of $a = 0.4594$ and $c = 0.2958$ nm [40]. There are six atoms in the unit cell, implying a total of 15 (= $3N − 3$) vibrational modes. The group theoretical analysis suggests that these 15 modes have the following irreduc-
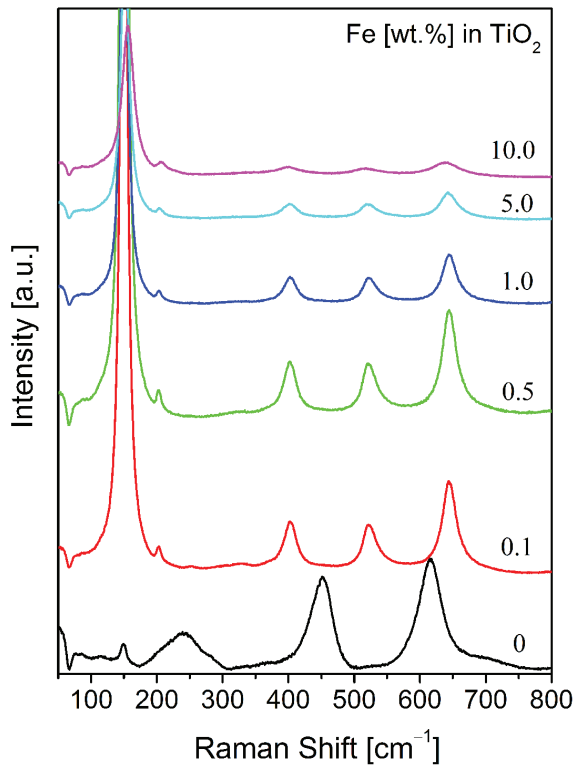
Figure 7. FT-Raman spectra of Fe-doped TiO₂ (with 0, 0.1, 0.5, 1, 5 and 10 wt.% Fe) powders formed at 550 °C for 6 h

ible representations: $A_{1g} + A_{2g} + A_{2u} + B_{1g} + B_{2g} + 2B_{1u} + E_g + 3E_u$. In which, the four modes, $A_{1g} + B_{1g} + B_{2g} + E_g$, are Raman active and four modes, $A_{2u} + 3E_u$, are infrared active. The other three modes, $A_{2g} + 2B_{1u}$, are neither Raman active nor infrared active. The frequencies of the Raman bands noted for pure rutile powder (i.e. for un-doped TiO₂) are at 141−157, 181−290, 415−479, 585−650 cm⁻¹ (Fig. 7). Balachandran and Eror [40] reported six frequencies at 144, 235, 320-360, 448, 612, and 827 cm⁻¹ for rutile titania. On the other hand, the conventional crystallographic unit cell of anatase TiO₂

is body centred tetragonal (space group D_{4h}^{14}, $I4_1/amd$, with an elongated cell having $a = 0.3783$ and $c = 0.951$ nm) and contains two primitive unit cells, each of which contains two formula units of TiO₂ [40]. According to the factor group analysis, six modes of anatase TiO₂, $A_{1g} + 2B_{1g} + 3E_g$ are Raman active and three modes, $A_{2u} + 2E_u$, are infrared active. One vibration, B_{2u}, will be inactive in both infrared and Raman spectra. All of these modes account for the 15 normal modes of vibration. Thus, group theory predicts six Raman active modes for the tetragonal anatase phase: three E_g modes centred around 145, 197, and 639 cm⁻¹; two B_{1g} modes at 399 and 519 cm⁻¹; and one A_{1g} mode at 513 cm⁻¹ [41]. The frequencies of the Raman bands noted for anatase TiO₂ (in the powders doped with 0.1, 0.5, 1, and 5 wt.% Fe) are at 108−188, 205, 387−425, 512−543, 625−670 cm⁻¹ (Fig. 7). In the literature Raman bands reported for anatase TiO₂ are at 146, 198, 320, 398,448, 515, 640, and 796 cm⁻¹ [40]. As mentioned above, the band at about 146 cm⁻¹ is the strongest of all the observed bands, and the bands at 198, and 640 cm⁻¹ are assigned to the E_g modes and the one at 401 cm⁻¹ to the B_{1g} mode. The doublet band at 522 cm⁻¹ is assigned to A_{1g} and B_{1g} modes [40]. These results are comparable with those reported for anatase and rutile phases of TiO₂ in the literature [42]. The α-Fe₂O₃ and TiFe₃O₄ seems to have exhibited no prominent Raman bands as the TiO₂ powders containing these phases did not reveal any other additional Raman peaks or bands.

The UV-Vis diffuse reflectance spectra (DRS) of the Fe-doped TiO₂ (with 0, 0.1, 0.2, 0.3, 0.4, 0.5, 0.6, 0.7, 0.8 and 0.9, and 1, 2, 3, 4, 5, 6, 7, 8, 9 and 10 wt.% Fe) powders calcined at 550 °C for 6 h are presented in Fig. 8. It can be seen that pure undoped (rutile) and the 0.1 wt.% Fe-doped TiO₂ powders (Fig. 8a) show absorption spectra consisting a single broad intense absorption at around 400 nm (i.e. in the UV range) occurred due to the charge-transfer (CT) from the valence band (mainly formed by 2p orbitals of the oxide anions) to the conduc-
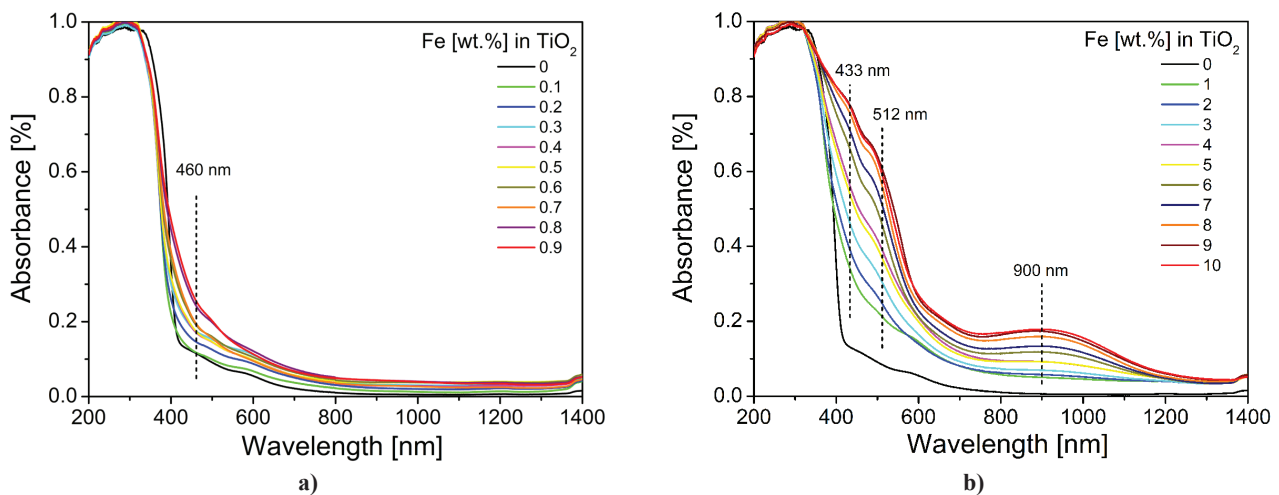

a)

b)

Figure 8. UV-Vis diffuse reflectance spectra (DRS) of: a) 0 to 0.9 wt.% and b) 0 to 10 wt.% Fe-doped TiO₂ powders formed at 550 °C for 6 h

tion band (mainly formed by 3d t$_{2g}$ orbitals of the Ti^{4+} cations) [43]. The 0.1 wt.% Fe-doped TiO$_2$ powder exhibited the spectra just like the one exhibited by P-25 TiO$_2$ (Degussa) powder [43]. The DRS spectra of 7 to 10 wt.% Fe-doped TiO$_2$ powders revealed three absorption bands in the wavelength ranges of 400−475 nm, 475−550 nm and 800−1100 nm (visible region) with three λ_{max} peaks at about 433 nm, 512 nm and 900 nm, respectively. The degree of absorbance of these latter peaks increased with the increase of Fe-content in TiO$_2$. The powders doped with >5 wt.% Fe exhibited the higher amounts of light absorbance (Fig. 8b). It has been reported that the doping of various transitional metal ions into TiO$_2$ could shift its optical absorption edge from UV into visible light range (i.e., red shift) [44]. Thus, these UV-Vis DRS results are in good agreement with those reported for Fe-doped TiO$_2$ powders in the literature [4,8,13−23,40−44].

In order to establish the type of band-to-band transition in the 0.1, 0.5, 1, 5 and 10 wt.% Fe-doped TiO$_2$ powders formed at 550 °C for 6 h, the absorbance data of DRS spectra was fitted into equations for both indirect and direct band gap transitions [39,40]. Figure 9a shows the $[F(R\infty)E]^2$ vs. E_{phot} plot for direct transition and Fig. 9b shows the $[F(R\infty)E]^{1/2}$ vs. E_{phot} plot for indirect transition. The Kubelka-Munk function $F(R\infty)$ is equivalent to absorbance in these UV-Vis DRS spectra

and E_{phot} is the photon energy, $E_{phot} = (1239/\lambda)$ eV, where λ is the wavelength in nm [33]. The value of E_{phot} extrapolated to $F(R\infty)E = 0$, which gives an absorption energy, corresponds to a band gap E_{bg} [32,33,38,39]. A close look at these graphs reveals that all these powders possess direct band gap transitions. The calculated E_{bg} values of these powders are presented in Table 2. It can be seen that as the Fe concentration increased in TiO$_2$, the band gap energy is gradually decreased, which is consistent with the red shift of absorption edge observed in DRS spectra (Fig. 8). These red shifts can be attributed to the charge transfer transitions between the metal ion d electrons and the conduction or valence band of TiO$_2$. Based on E_{bg} and absorption edge values noted, the pure TiO$_2$ is expected to be active under UV irradiation, whereas, the Fe-doped TiO$_2$ (with 0.1, 0.5, 1, 5 and 10 wt.% Fe) powders under visible light [8].

In order to find out whether a shift of the valence or conduction band edge is responsible for the decrease of the band gap energy of TiO$_2$ with the increase of Fe-doping concentration, the position of the quasi-Fermi level of electrons ($_nE_F^*$) (i.e., the flat-band potential values, U_{fb}) were determined by measuring the photovoltages of Fe-doped TiO$_2$ powders as a function of the suspension pH value (Fig. 10). From the pH value of the inflection point (pH_0), the quasi-Fermi level at pH=7 could be calculated
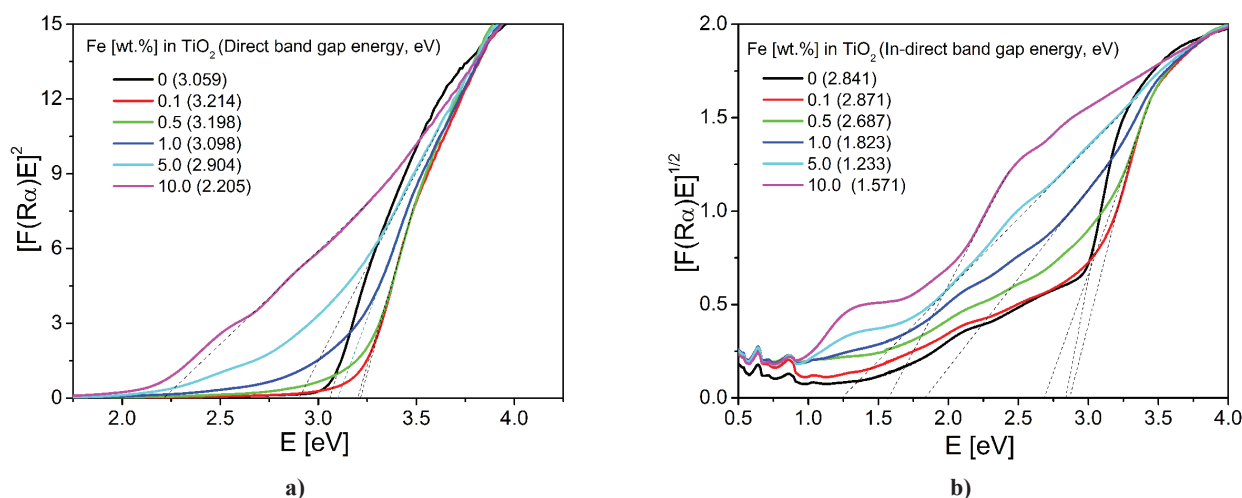

Figure 9. Transformed diffuse reflectance spectra of Fe-doped TiO$_2$ (with 0, 0.1, 0.5, 1, 5 and 10 wt.% Fe) powders formed at 550 °C for 6 h showing: a) direct band gap and b) indirect band gap energy values

Table 2. Photoelectrochemical and band gap energy data of 0.1, 0.5, 1, 5 and 10 wt.% Fe-doped TiO$_2$ powders formed at 550 °C for 6 h[†]

Fe in TiO$_2$ [wt.%]	Zeta potential (mV) at pH=7	pH_0[a]	E_{bg} [eV][b]		U_{fb} (vs. NHE)[a] calculated for pH~7 [V][c]
			Direct	Indirect	
0.1	−40.1±3.90	6.6	3.214	2.871	−0.2696
0.5	−48.8±2.78	5.5	3.198	2.687	−0.3345
1	−49.5±4.06	4.4	3.098	1.823	−0.3994
5	−49.8±2.95	3.6	2.904	1.233	−0.4466
10	−52.9±2.95	2.7	2.205	1.571	−0.4997

[†]The values are arrived as detailed in the experimental section.
[a] Measured according to ref. [32,33]. [b] These values measured for powders by following DRS spectra, and the reproducibility was better than ±0.01 eV. [c] Reproducibility was better than ±0.01 V.
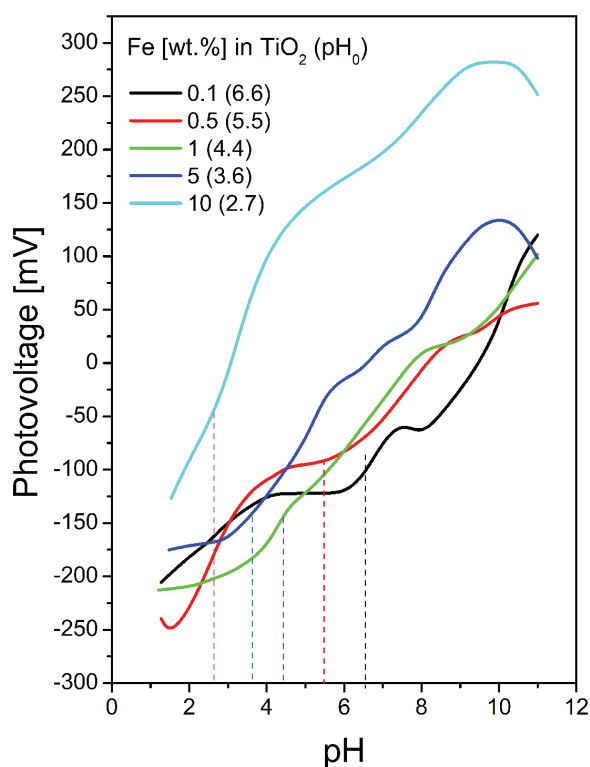
Figure 10. Dependence of photovoltage (V vs. Ag/AgCl) of Fe-doped TiO₂ (with 0.1, 0.5, 1, 5 and 10 wt.% Fe) powders formed at 550 °C for 6 h on pH of electrolyte

(Table 2) [32,33]. An increase in Fe-dopant concentration has caused an increasing trend in the flat band potentials (U_{fb}). These values increased from −0.2696 V for the 0.1 wt.% Fe-doped TiO₂ to −0.4997 V for the 10 wt.% Fe-doped TiO₂. This change in the flat band potential could be attributed to the various modifications such as, change in the crystallite size and specific surface area, the formation of certain additional secondary phases, etc., occurred to the TiO₂ powders upon doping with Fe. A value of −0.52 V for TiO₂ at pH=7 measured by slurry meth-

od [33], −0.58 V for an anatase single crystal measured by Mott-Schottky method [45] and −0.47 V for anatase powder also measured by slurry method [46] were reported in the literature. The values measured in the present study are slightly different from those values reported in the literature already [32,33]. These differences could be attributed to the presence of Fe in TiO₂ and to the differences in their methods of preparation. Assuming that the distance between the quasi-Fermi level of electrons and the conduction band edge is decreasing with the increase of Fe in TiO₂, one could locate the position of the valence band edge by adding the band gap energy to the quasi-Fermi level value [32,33]. Potential values of 2.944, 2.863, 2.758, 2.457, and 1.705 V (vs. NHE) for the 0.1, 0.5, 1, 5, and 10 wt.% Fe-doped TiO₂ powders could be calculated at pH=7 (Fig. 11). These measured flat band potentials and band gap energy values suggest that these synthesized Fe-doped TiO₂ powders are probable candidate members of choice for artificial photosynthesis reactions (i.e., for photo-electrolysis of water into hydrogen and oxygen gases).

Table 2 also lists the measured values of zeta potentials (ζ) of the 0.1, 0.5, 1, 5 and 10 wt.% Fe-doped TiO₂ powders formed at 550 °C for 6 h. It can be seen that there is a gradual increase in the zeta-potential values of TiO₂ from −40.1 ± 3.90 mV to −52.9 ± 2.95 mV with the increase of Fe-dopant concentration from 0.1 to 10 wt.% in TiO₂. The iso-electric point of TiO₂ lies in pH less than 6.8 [46,47]. The solution at pH=7 renders TiO₂ powder surface a negative charge, resulting in negative ζ values. The change of ζ values with increase of Fe-content suggests that the isoelectric point of TiO₂ powder is changing with the increase of Fe concentration in it. Development of charge on TiO₂ powder surface in aqueous medium can be shown with equations (3) and (4):

$$Ti\text{-}OH + H^+ \leftrightarrow Ti\text{-}OH_2^+ \qquad (3)$$

$$Ti\text{-}OH + \text{-}OH^- \leftrightarrow Ti\text{-}O^- + H_2O \qquad (4)$$

It is generally accepted that the surface of the TiO₂ powder exists in the form of TiOH groups. These hydroxyl groups dissociate into water and confer to the particles a surface charge as shown in equations (3) and (4). These equations further suggest that the solution pH also possesses a strong influence on the surface catalytic reactions of TiO₂ powders in aqueous medium. Since, these powders possess negative zeta potentials, it is expected that the reactions of organic molecules/reactants having positive charge would be higher on the surfaces of these Fe-doped TiO₂ powders [46,47].

The methylene blue (MB) degradation experiments in water under the irradiation of simulated solar light were conducted to assess the photocatalytic efficiency of 0.1, 0.5, 1, 5 and 10 wt.% Fe-doped TiO₂ powders. Figure 12 shows the C/C_0 of 0.01, 0.02 and 0.03 mM aqueous MB solutions, respectively, irradiated with simulated so-
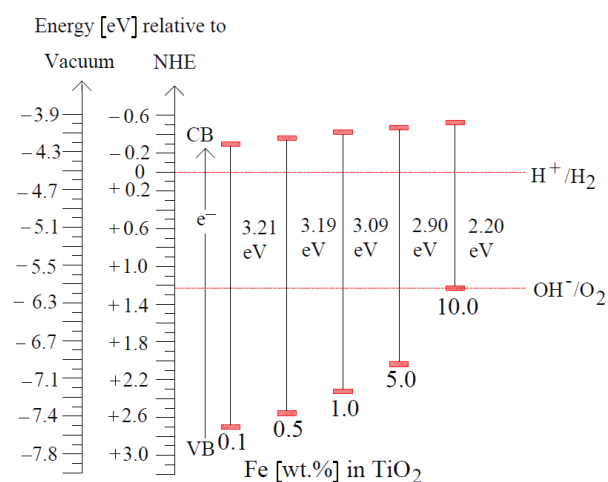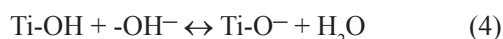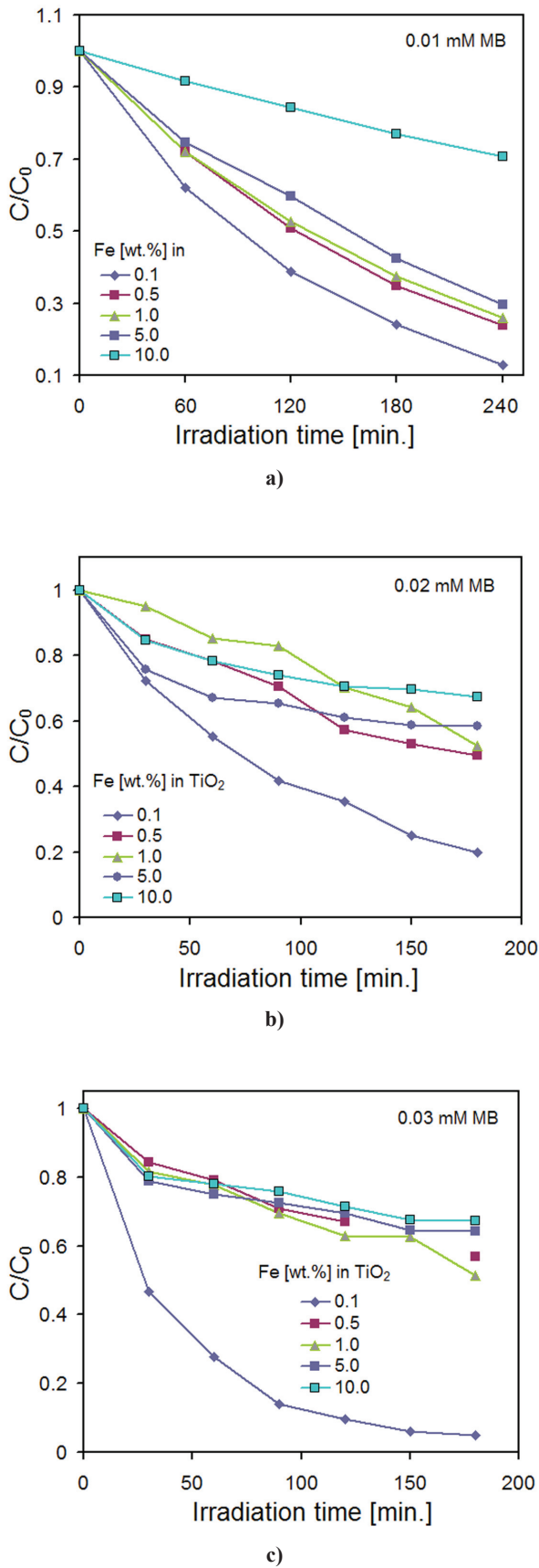

Figure 11. The electrochemical potentials (vs. NHE) of band edges of Fe-doped TiO₂ (with 0.1, 0.5, 1, 5 and 10 wt.% Fe) powders (formed at 550 °C for 6 h) at pH 7

lar light over different amounts of Fe-doped TiO$_2$ powders as a function of reaction time. It can be seen that among the five powders tested, only the 0.1 wt.% Fe-doped TiO$_2$ powder showed the highest photocatalytic activity and as the concentration of Fe increased in TiO$_2$, the photocatalytic efficiency was gradually decreased. Furthermore, the photocatalytic efficiency of these catalysts was also decreased with the increase of MB concentration in the aqueous reaction solution. The UV-visible spectra revealing the degradation behaviour of 0.03 mM MB solution over the 1 wt.% Fe-doped TiO$_2$ powder as a function of reaction time is shown in Fig. 13. In order to assess the rate of photocatalytic degradation of MB over the 0.1, 0.5, 1, 5 and 10 wt.% Fe-doped TiO$_2$ powders, the observed MB degradation results were kinetically analyzed by following Langmuir-Hinshelwood rate constant equations [14,48]. Langmuir-Hinshelwood (Eq. (5)) described the relationship between the initial degradation rate (r) and the initial concentration (C) of the organic substrate for heterogeneous photocatalytic degradation [14,48]. The model can be written as follows:

$$r = \frac{-dC}{dt} = \frac{kK_{ads}C}{1 + K_{ads}C} = k_{obs}C \qquad (5)$$

where:

$$k_{obs} = \frac{kK_{ads}}{1 + K_{ads}C} \qquad (6)$$

$$\frac{1}{k_{obs}} = \frac{1}{kK_{ads}} + \frac{C}{k} \qquad (7)$$

$$-\ln\frac{Ct}{Co} = k_{obs}\,t \qquad (8)$$

C_o (ppm) is the initial concentration of MB, C_t (ppm) is the remaining concentration after t (h) time irradiation, K_{ads} is the Langmuir-Hinshelwood adsorption
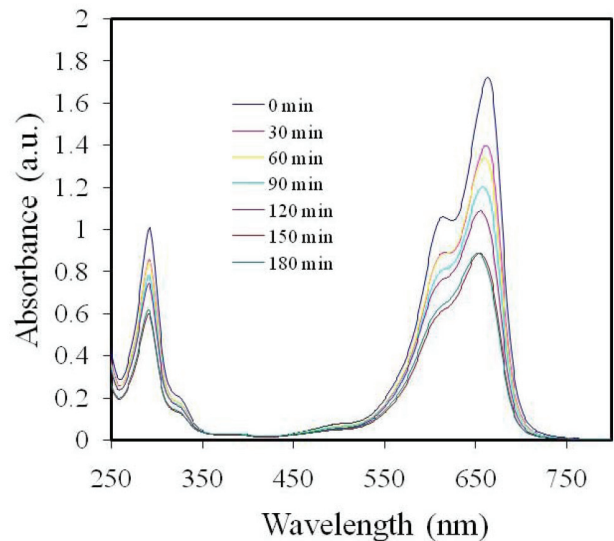

Figure 12. Effect of the concentration of methylene blue (MB) on photocatalytic ability of Fe-doped TiO$_2$ (with 0.1, 0.5, 1, 5 and 10 wt.% Fe) powders formed at 550 °C for 6 h. (a) 0.01 mM; (b) 0.02 mM and (c) 0.03 mM MB solutions

Figure 13. The UV-visible spectra of 0.03 mM MB solution irradiated with simulated solar light of 44 mW/cm^2 over 1 wt.% Fe-doped TiO$_2$ powder for different time intervals

Table 3. The initial concentrations and the pseudo-first order rate constant (k) of methylene blue degradation under the irradiation of simulated solar light over 0.1, 0.5, 1, 5 and 10 wt.% Fe-doped TiO₂ powders formed at 550 °C for 6 h[†]

Fe in TiO$_2$ [wt.%]	C_0 of MB [ppm]	k_{obs} [h^{-1}] (±0.020)	K_{ads}	k [ppm h^{-1}] (×10^{-2})
	3.198 (0.01 mM)	0.494		
0.1	6.397 (0.02 mM)	0.017	0.266	5.865
	9.595 (0.03 mM)	0.009		
	3.198	0.352		
0.5	6.397	0.015	0.274	2.590
	9.595	0.004		
	3.198	0.331		
1	6.397	0.011	0.291	2.588
	9.595	0.004		
	3.198	0.291		
5	6.397	0.009	0.369	1.309
	9.595	0.002		
	3.198	0.086		
10	6.397	0.003	1.082	1.288
	9.595	0.002		

[†]The values are arrived as detailed in the experimental section
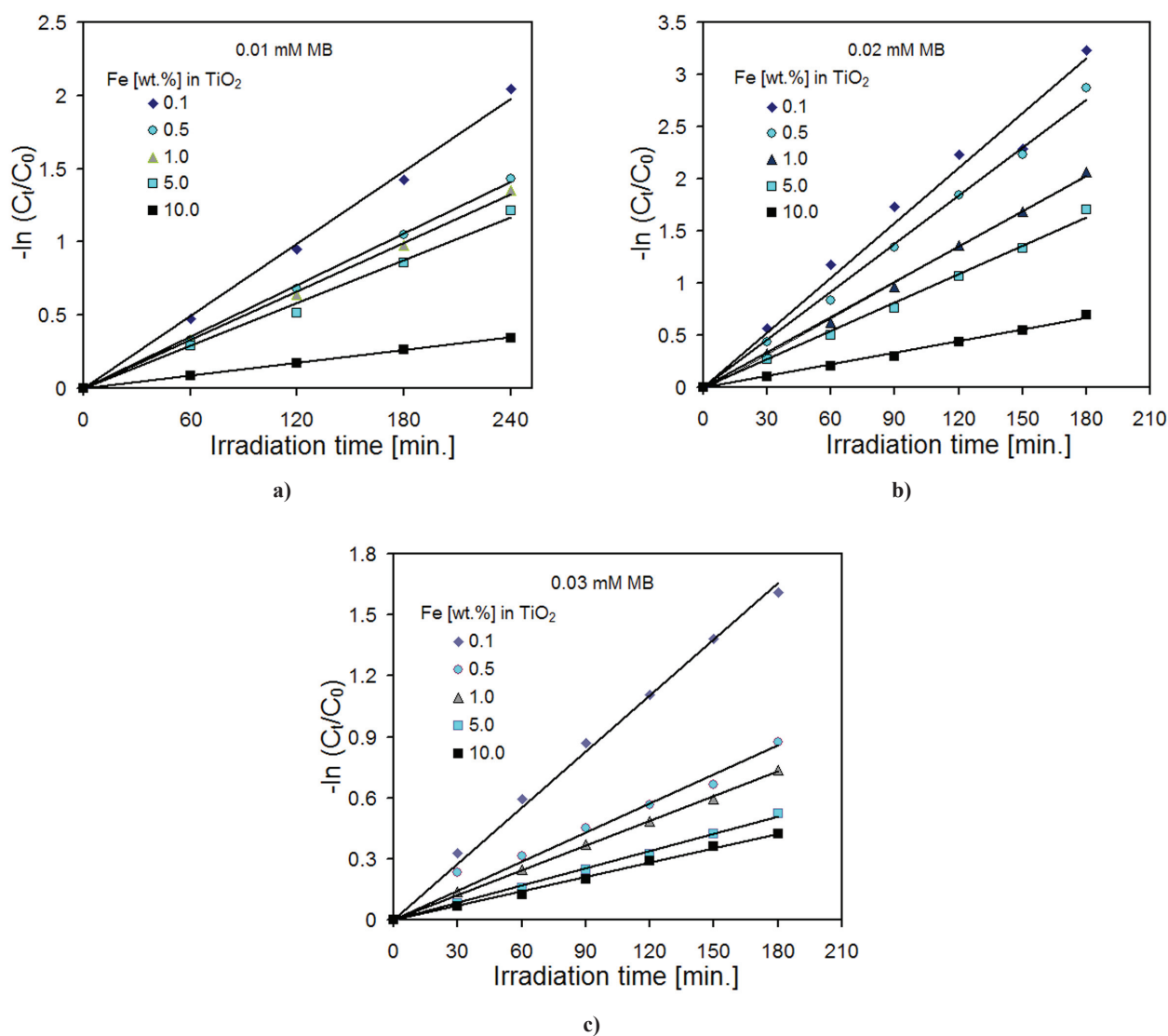

a)

b)

c)

Figure 14. Linear transforms: –ln (C$_t$/C$_o$) versus irradiation time for methylene blue (MB) under simulated solar light over Fe-doped TiO$_2$ (with 0.1, 0.5, 1, 5 and 10 wt.% Fe) powders formed at 550 °C for 6 h. (a) 0.01 mM; (b) 0.02 mM and (c) 0.03 mM MB solutions

equilibrium constant (ppm^{-1}), and k is the pseudo-first order rate constant relating to TiO$_2$ surface reaction (ppm h^{-1}).

The k observed (k_{obs}) values for each initial concentration were estimated from the slopes of straight line obtained by plotting $-\ln(C_t/C_0)$ *vs.* irradiation time as shown in Fig. 14 and Table 3. By plotting initial concentrations *vs.* $1/k_{obs}$, the rate constant (k) and the adsorption equilibrium constant K_{ads} were calculated. Equation (7) can be identified as $Y = m \cdot X + C$, where, $C = 1/(k \cdot K_{ads})$, $m = 1/k$, $Y = 1/k_{obs}$ and X is the initial concentration (C_0) of MB. By using the Eq. (5) and the data of Table 3, the initial degradation rates (r) of MB over Fe-doped TiO$_2$ powders were calculated. It can be clearly seen that the Langmuir-Hinshelwood adsorption equilibrium constant and the rate constant values suggest that the 0.1 wt.% Fe-doped TiO$_2$ powder shows the highest photo-catalytic activity for MB degradation under the irradiation of simulated solar light. The data of Figs. 12 and 14 suggests that the TiO$_2$ powder doped with 0.1 wt.% Fe exhibits the highest photocatalytic ability for MB degradation under the irradiation of simulated solar light.

IV. Conclusions

The following conclusions can be drawn from the above study:

1. Chemically homogeneous and fully crystalline Fe-doped TiO$_2$ (with 0 to 10 wt.% Fe) powders can be prepared following a co-precipitation method. The TiO$_2$ powder formed from TiCl$_4$ in a co-precipitation route exists in the form of crystal pure rutile phase, whereas, the TiO$_2$ powder doped with Fe (up to 10 wt.%) exists in the form of anatase phase.

2. Even 0.1 wt.% Fe is sufficient to transform TiO$_2$ from fully rutile to fully anatase phase and to enhance TiO$_2$ powders specific surface area from 23.25 to 65.92 m^2/g. The Fe-dopant confers a red shift to light absorbing capability of TiO$_2$ and reduces its band gap energy considerably.

3. Both undoped and Fe-doped TiO$_2$ powders possess direct band gap energy transitions.

4. Among various Fe-doped TiO$_2$ powders, the one doped with 0.1 wt.% Fe shows the highest photocatalytic activity for methylene blue (MB) degradation under the irradiation of simulated solar light. The Fe-doped TiO$_2$ powders follow the Langmuir-Hinshelwood first order reaction rate constant relationship in the photocatalytic MB degradation reactions.

5. The Fe-doped TiO$_2$ powders possess flat band potentials suitable for artificial photosynthesis reactions. Though, Fe$_2$O$_3$ is a *p*-type semi-conducting material, the Fe-doped TiO$_2$ materials exhibit *n*-type semi-conducting behaviour.

References

1. M. Halmann, "Photoelectrochemical reduction of aqueous carbon-dioxide on p-type gallium-phosphide in liquid junction solar cells", *Nature*, **275** (1978) 115–116.
2. E.E. Barton, D.M. Rampulla, A.B. Bocarsly, "Selective solar-driven reduction of CO$_2$ to methanol using a catalyzed *p*-GaP based photoelectrochemical cell", *J. Am. Chem. Soc.*, **130** [20] (2008) 6342–6344.
3. K.W. Jr. Frese, S.C. Leach, D.P. Summers, "Electrochemical reduction of aqueous carbon dioxide to methanol", *U.S. Patent No.* 4,609,441, dated: 2nd September 1986.
4. A. Fujishima, K. Honda, "Electrochemical photolysis of water at a semiconductor electrode", *Nature*, **238** (1972) 37–40.
5. M. Gratzel, "Photoelectrochemical cells", *Nature*, **414** [6861] (2001) 338–344.
6. K. Ohashi, J. Mc Cann, J.O.M. Bockris, "Stable photoelectrochemical cells for splitting of water", *Nature*, **266** [5603] (1977) 610–611.
7. S. Licht, "A description of energy-conversion in photoelectrochemical solar-cells", *Nature*, **330** [6144] (1987) 148–151.
8. T. Bak, J. Nowotny, M. Rekas, C.C. Sorrell, "Review article: Photo-electrochemical hydrogen generation from water using solar energy: materials-related aspects", *Inter. J. Hydrogen Energy*, **27** (2002) 991–1022.
9. I. Ganesh, "Conversion of carbon dioxide to methanol using solar energy – a brief review", *Mater. Sci. Applic.*, **2** [10] (2011) 1407–1415.
10. I. Ganesh, "An opinion on conversion of carbon dioxide to methanol using solar energy", *Curr. Sci.*, **101** [6] (2011) 731–733.
11. A.J. Nozik, "p-n photoelectrolysis cell", *Appl. Phys. Lett.*, **29** (1976) 150–153.
12. A.J. Nozik, "Photochemical diodes", *US Patent No.*: 4,094,751, June 13, 1978.
13. Y.J. Lin, Y.H. Chang, W.D. Yang, B.S. Tsai, "Synthesis and characterization of ilmenite NiTiO$_3$ and CoTiO$_3$ prepared by a modified Pechini method", *J. Non-Crystal. Solids*, **352** (2006) 789–794.
14. I. Ganesh, A.K. Gupta, P.P. Kumar, P.S.C. Sekhar, K. Radha, G. Padmanabham, G. Sundararajan, "Preparation and characterization of Ni-doped TiO$_2$ materials for photocurrent and photocatalytic applications", *Sci. World J.*, in press, 2012.
15. I. Ganesh, A.K. Gupta, P.P. Kumar, P.S.C. Sekhar, K. Radha, G. Padmanabham, G. Sundararajan, "Preparation and characterization of Co-doped TiO$_2$ materials for solar light induced current and photocatalytic applications", *Mater. Chem. Phys.*, in press, 2012.

16. S. Kumari, Y.S. Chaudhary, S.A. Agnihotry, C. Tripathi, A. Vermac, D. Chauhan, R. Shrivastav, S. Dass, V.R. Satsangia, "A photoelectrochemical study of nano-structured Cd-doped titanium oxide", *Inter. J. Hydrogen Energy*, **32** (2007) 1299–1302.

17. J.A. Navio, M. Macias, M. Gonzalez-Catalan, A. Justo, "Bulk and surface characterization of powder iron-doped titania photocatalysts", *J. Mater. Sci.*, **27** (1992) 3036–3042.

18. M.I. Litter, J.A. Navio, "Photocatalytic properties of iron-doped titania semiconductors", *J. Photochem. Photobiol. A Chem.*, **98** [3] (1996) 171–181.

19. R.I. Bickley, J.S. Lees, R.J.D. Tilley, L. Palmisano, M. Schiavello, "Characterization of iron/titanium oxide photocatalysts: part 1 - structural and magnetic studies", *J. Chem. Soc., Faraday Trans.*, **88** (1992) 377–383.

20. D. Cordishi, N. Burriesci, F.D. Alba, M. Petrera, G. Polizzotti, M. Schiavello, "Structural characterization of Fe/Ti oxide photocatalysts by X-ray, ESR, and Mossbauer methods", *J. Solid State Chem.*, **56** (1985) 182–190.

21. M.V. Tsodikov, O.V. Bukhtenko, O.G. Ellert, V.M. Shcherbakov, D.I. Kochubey, "Low-temperature formation mechanism of double oxides $Fe_xZr(Ti)_{1-075x}O_{2-\delta}$ prepared from alkoxides and acetylacetonates", *J. Mater. Sci.*, **30** [4] (1995) 1087–1094.

22. Y. Wang, H. Cheng, Y. Hao, J. Ma, W. Li, S. Cai, "Preparation, characterization and photoelectrochemical behaviours of Fe (III)-doped TiO_2 nanoparticles", *J. Mater. Sci.*, **34** (1999) 3721–3729.

23. A.R. Ballyy, E.N. Korobeinikova, P.E. Schmid, F. Levy, F. Bussy, "Structural and electrical properties of Fe-doped TiO_2 thin films", *J. Phys. D: Appl. Phys.*, **31** (1998) 1149–1154.

24. U. Jorskten, J. Moser, M. Gratzel, "Photoelectrochemical studies on nanocrystalline hematite films", *Chem. Mater.*, **6** (1994) 858–863.

25. G.S. Nahor, L.C.T. Shoute, P. Neta, A. Harriman, "Reduction of dinitrogen to ammonia in aqueous solution mediated by colloidal metals", *J. Chem. Soc., Faraday Trans.*, **86** (1990) 3927–3933.

26. V. Augugliaro, A. Laurucella, L. Rizzuti, M. Schiavello, A. Sclafani, "Conversion of solar energy to chemical energy by photoassisted processes. I: Preliminary results on ammonia production over doped titanium dioxide catalysts in a fluidized bed reactor", *Int. J. Hydrogen Energy*, **7** [11] (1982) 845–849.

27. K.T. Ranjit, B. Vishwanathan, "Synthesis, characterization and photocatalytic properties of iron-doped TiO_2 catalysts", *J. Photochem. Photobio. A: Chem.*, **108** (1997) 79–84.

28. A.P. Singh, S. Kumari, R. Shrivastav, S. Dass, V.R. Satsangi, "Iron doped nanostructured TiO_2 for photoelectrochemical generation of hydrogen", *Int. J. Hydrogen Energy*, **33** (2008) 5363–5368.

29. B.M. Reddy, I. Ganesh, "Characterization of La_2O_3–TiO_2 and V_2O_5/La_2O_3–TiO_2 catalyst and their activity for synthesis of 2,6-dimethylphenol", *J. Mol. Catal. A: Chemical*, **169** (2001) 207–223.

30. B.M. Reddy, I. Ganesh, E.P. Reddy, A. Fernández, P.G. Smirniotis, "Surface characterization of Ga_2O_3-TiO_2 and V_2O_5/Ga_2O_3-TiO_2 catalysts", *J. Phys. Chem. B*, **105** (2001) 6227–6235.

31. R.J. Tayade, T.S. Natarajan, H.C. Bajaj, "Photocatalytic degradation of methylene blue dye using ultraviolet light emitting diodes", *Ind. Eng. Chem. Res.*, **48** (2009) 10262–10267.

32. A.M. Roy, G.C. De, N. Sasmal, S.S. Bhattacharyya, "Determination of the flat band potential of semiconductor particles in suspension by photovoltage measurement", *Int. J. Hydrogen Energy*, **20** (1995) 627–630.

33. H. Kisch, S. Sakthivel, M. Janczarek, D. Mitoraj, "A low-bandgap, nitrogen modified titania visible light photocatalyst", *J. Phys. Chem. C*, **111** (2007) 11445–11449.

34. W.D. Kingery, H.K. Bowen, D.R. Uhlman, *Introduction to Ceramics*, 2nd ed. Wiley, New York, 1976.

35. H.P. Klug, L.E. Alexander, "X-ray diffraction procedures for polycrystalline and amorphous materials", *J. Appl. Crystallogr.*, **8** (1975) 573–574.

36. P. Jones, J.A. Hockey, "Infra-red studies of rutile surfaces: part 1", *Trans Faraday Soc.*, **67** (1971) 2669–2678.

37. H.P. Boem, "Chemical identification of surface groups", *Adv. Cat.*, **16** (1966) 179–274.

38. J. Tauc, *Amorphous and Liquid Semiconductors*. Ed. J. Tauc, Plenum Press, New York, 1976, 609–705.

39. J. Tauc, A. Menth, "State in the gap", *J. Non Crystal. Solids*, **8-10** (1972) 569–585.

40. U. Balachandran, N.G. Eror, "Raman spectra of titanium dioxide", *J. Solid State Chem.*, **42** (1982) 276–282.

41. M. Mikami, S. Nakamura, O. Kitao, H. Arakawa, "Lattice dynamics and dielectric properties of TiO_2 anatase: a first-principles study", *Phys. Rev. B: Condensed Matter Mater. Phys.,* **66** (2002) 155–213.

42. M.I. Baraton, G. Busca, M.C. Prieto, G. Ricchiardi, V.S. Escribano, "On the vibrational spectra and structure of $FeCrO_3$ and of the ilmenite-type compounds $CoTiO_3$ and $NiTiO_3$", *J. Solid State Chem.*, **112** (1994) 9–14.

43. N. Venkatachalam, M. Palanichamy, V. Murugesan, "Sol-gel preparation and characterization of nanosize TiO_2: its photocatalytic performance", *Mater. Chem. Phys.*, **104** [2-3] (2007) 454–459.

44. J.C.S. Wu, C.H. Chen, "A visible-light response vanadium-doped titania nanocatalyst by sol-gel method", *J. Photochem. Photobiol. A*, **163** (2004) 509–515.

45. C.A. Hogarth, Z.T. Al-Dhhan, "Optical absorption in thin films of cerium dioxide and cerium dioxide containing silicon monoxide", *Phys. Status Sol. B*, **137** (1986) K157–K160.

46. L. Kavan, M. Gratzel, S.E. Gilbert, C. Klemenz, H.J. Scheel, "Electrochemical and photoelectrochemical investigation of single-crystal anatase", *J. Am. Chem. Soc.*, **118** [28] (1996) 6716–6723.

47. M.D. Ward, J.R. White, A.J. Bard, "Electrochemical investigation of the energetics of particulate titanium dioxide photocatalysts: the methyl viologen-acetate system", *J. Am. Chem. Soc.*, **105** [1] (1983) 27–31.

48. G.J. Cunningham, G. Al-Sayyed, S. Srijaranai, *Aquatic and Surface Photochemistry*. Eds. G.R. Helz, R.G. Zepp, D.G. Grosby, Lewis Publisher, Boca Raton, 1994, p. 317.